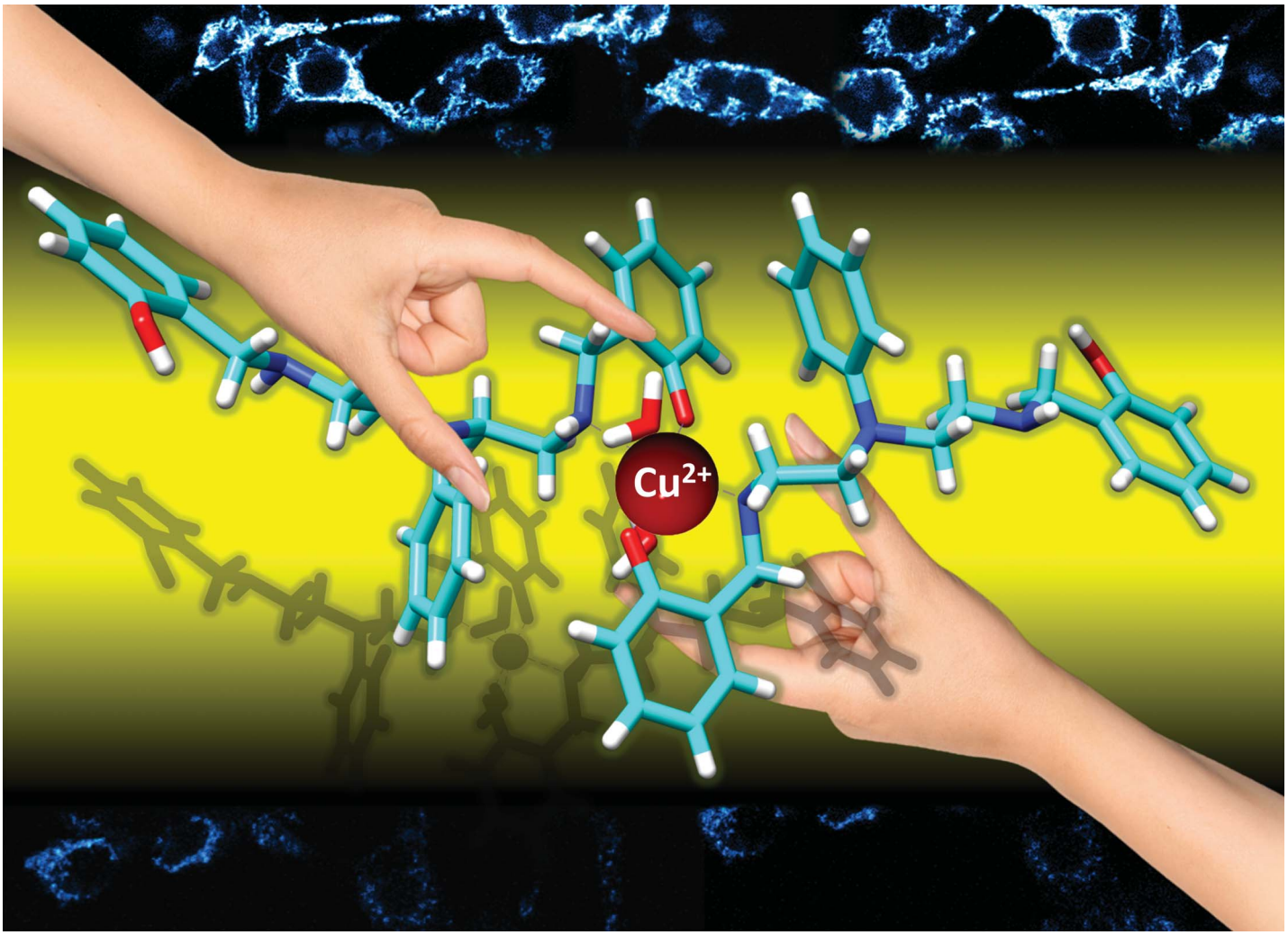

Showcasing research from Dr. Ankona Datta's laboratory, Department of Chemical Sciences, Tata Institute of Fundamental Research, Mumbai, India.

Cu^{2+} selective chelators relieve copper-induced oxidative stress *in vivo*

Cu^{2+} selective chelators exhibit 10^8 times higher conditional stability constants toward Cu^{2+} over Cu^{+} and other biologically relevant metal ions. The chelators specifically remove excess Cu^{2+} ions from living cells and alleviate Cu induced oxidative stress all the way from Menkes disease model cells of Cu overload to a live multicellular vertebrate system. The unique selectivity of our chelators indicates tremendous potential in minimizing side-effects associated with non-specific Cu ion chelation based therapy currently used treat severe neurological and metabolic disorders like, Wilson's disease, amyotrophic lateral sclerosis, and Alzheimer's disease.

As featured in:

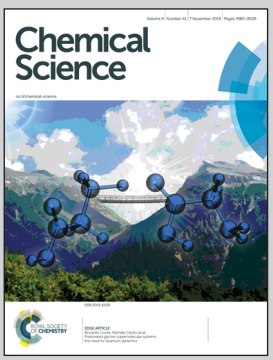

See Ankona Datta *et al.*, *Chem. Sci.*, 2018, **9**, 7916.

ROYAL SOCIETY OF CHEMISTRY

rsc.li/chemical-science

Registered charity number: 207890

Chemical Science

EDGE ARTICLE

View Article Online
View Journal | View Issue

Cite this: *Chem. Sci.*, 2018, **9**, 7916

All publication charges for this article have been paid for by the Royal Society of Chemistry

Cu^{2+} selective chelators relieve copper-induced oxidative stress *in vivo*†

Ananya Rakshit,[a] Kaustav Khatua,[a] Vinit Shanbhag,[b] Peter Comba[c] and Ankona Datta*[a]

Copper ions are essential for biological function yet are severely detrimental when present in excess. At the molecular level, copper ions catalyze the production of hydroxyl radicals that can irreversibly alter essential bio-molecules. Hence, selective copper chelators that can remove excess copper ions and alleviate oxidative stress will help assuage copper-overload diseases. However, most currently available chelators are non-specific leading to multiple undesirable side-effects. The challenge is to build chelators that can bind to copper ions with high affinity but leave the levels of essential metal ions unaltered. Here we report the design and development of redox-state selective Cu ion chelators that have 10^8 times higher conditional stability constants toward Cu^{2+} compared to both Cu^+ and other biologically relevant metal ions. This unique selectivity allows the specific removal of Cu^{2+} ions that would be available only under pathophysiological metal overload and oxidative stress conditions and provides access to effective removal of the aberrant redox-cycling Cu ion pool without affecting the essential non-redox cycling Cu^+ labile pool. We have shown that the chelators provide distinct protection against copper-induced oxidative stress *in vitro* and in live cells *via* selective Cu^{2+} ion chelation. Notably, the chelators afford significant reduction in Cu-induced oxidative damage in Atp7a$^{-/-}$ Menkes disease model cells that have endogenously high levels of Cu ions. Finally, *in vivo* testing of our chelators in a live zebrafish larval model demonstrate their protective properties against copper-induced oxidative stress.

Received 11th September 2018
Accepted 29th September 2018

DOI: 10.1039/c8sc04041a

rsc.li/chemical-science

1. Introduction

Redox-active metal ions are critical for biological function. Copper (Cu), iron (Fe), and manganese (Mn) ions act as co-factors for essential enzymes. Recent reports show that labile or weakly bound pools of redox active metal ions also participate in neuronal signaling and removal of reactive oxygen species.[1–4] While absolutely essential for biological activity both in protein-bound and labile forms, excess redox-active metal ions have been associated with severe neuro-degenerative disorders.[5–8] A significant route by which excess redox-active metal ions affect cellular function is *via* the Fenton reaction.[9–13] Cu^+/Cu^{2+} and Fe^{2+}/Fe^{3+} catalyze the production of reactive hydroxyl radicals which cause permanent modification of cellular lipids, nucleic acids, and proteins leading to severe oxidative damage (Fig. 1A and B).[9,10,12,14–16] Previous studies have shown that metal ion chelators can alleviate oxidative stress associated symptoms of metal-induced disorders.[17–23] However, a major shortcoming of chelation therapy is the non-specific removal of other biologically essential metal ions and metal co-factors from metallo-enzymes leading to multiple side-effects.[12,24–28] Therefore, cell-permeable metal selective chelators that can specifically remove excess metal ions responsible for oxidative stress would be extremely valuable motifs for chelation therapy (Fig. 1C).

We have worked on the development of selective cell-permeable chelators for redox-active metal ions with a focus on Cu ion chelation. The motivation for our work derives from the fact that while Cu^+/Cu^{2+} ions are absolutely essential for biological activity, abnormal Cu homeostasis is implicated in severe neurological and metabolic disorders like Alzheimer's disease,[7,29–32] amyotrophic lateral sclerosis,[33–37] cancer,[38,39] Menkes disease,[5,40,41] and Wilson's disease.[8,42–44]

Intra-cellular Cu ions are tightly regulated such that 'free' Cu^+–aqua species are almost non-existent.[45–49] Labile Cu ions are mostly bound to available biological ligands like glutathione and exist in the Cu^+ oxidation state under the normal reducing physiological conditions.[50,51] These 'natural' ligands tune the reduction potential of Cu such that the physiologically available

[a]*Department of Chemical Sciences, Tata Institute of Fundamental Research, 1 Homi Bhabha Road, Colaba, Mumbai-400005, India. E-mail: ankona@tifr.res.in*

[b]*Department of Biochemistry, Christopher S. Bond Life Science Center, University of Missouri, Columbia, USA*

[c]*Universität Heidelberg, Anorganisch-Chemisches Institut, Interdisciplinary Center for Scientific Computing, INF 270, D-69120 Heidelberg, Germany*

† Electronic supplementary information (ESI) available: Supporting figures and tables, details of LC methods for stability and purity analysis of chelators, ESI-MS spectrum of copper complexes, Job's plot, absorbance data and stability constant determination with different metal ions, EPR spectra, control experiments in cells and zebrafish larvae, and ^{1}H NMR, ^{13}C NMR are included. See DOI: 10.1039/c8sc04041a

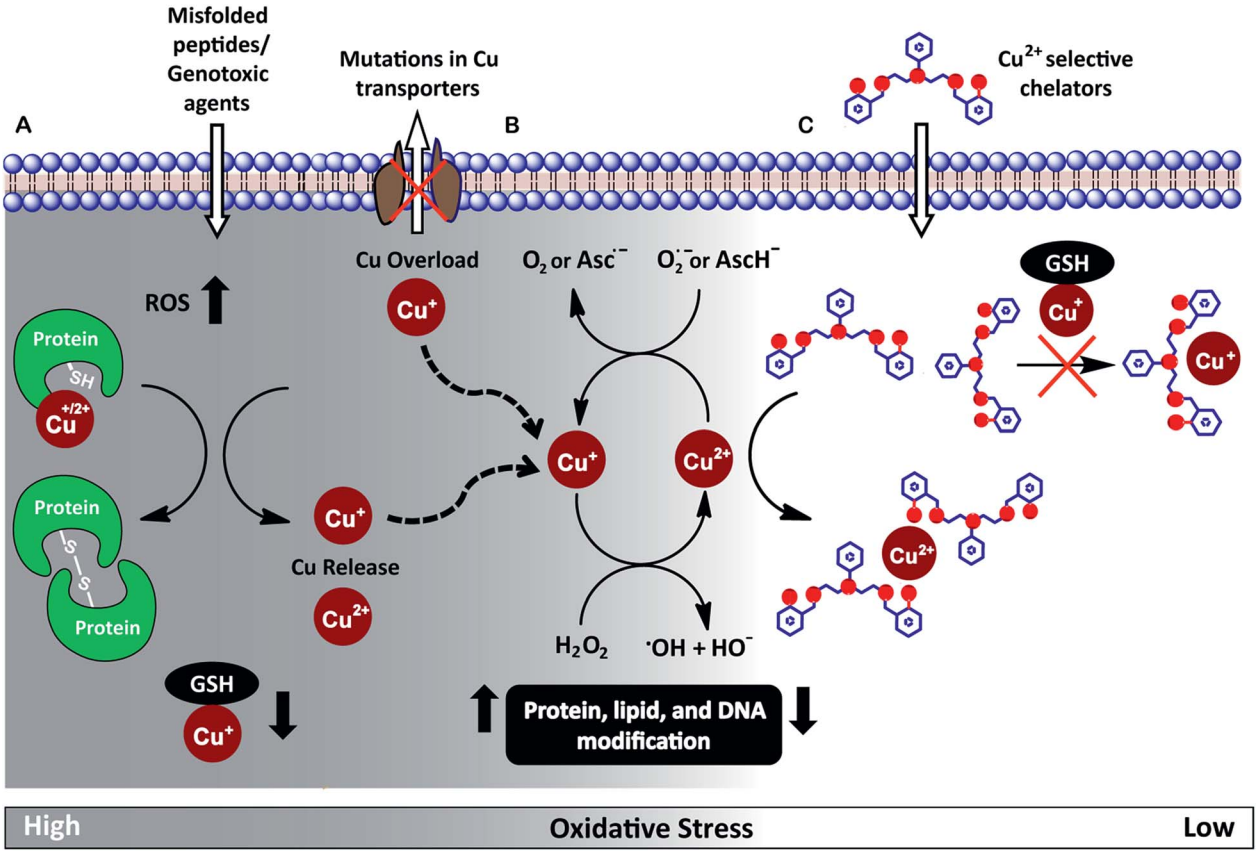

Fig. 1 (A) Scheme highlighting mechanisms that can increase intracellular Cu ion levels. Exposure to external agents and mis-folded peptides can cause increased levels of reactive oxygen species (ROS) leading to oxidative stress. Increased oxidative stress leads to protein oxidation releasing Cu ions from proteins and also reduces levels of glutathione (GSH) bound Cu^{+}. Mutations in Cu ion transporters lead to elevated intracellular Cu ion levels. (B) Cu^{+}/Cu^{2+} catalyzed Fenton reaction produces reactive hydroxyl radicals, $HO^{\bullet}$. Cu^{2+} is reduced by cellular reductants like superoxide ($O_2^{\bullet-}$) and hydroascorbate ($AscH^{-}$) to complete the catalytic cycle. (C) Proposed cell-permeable Cu^{2+} chelators that alleviate oxidative stress *via* selective Cu^{2+} chelation.

labile pool does not participate in Fenton chemistry and the cell is able to efficiently regulate Cu ions to minimize oxidative damage.[12,13,52] However, the Cu balance gets compromised during disease conditions *via* multiple mechanisms leading to Cu ion overload (Fig. 1A).[5,13,35,36,41,43,52] Under Cu dysregulation conditions, excess Cu ions can bind to other biologically available ligands and misfolded proteins forming copper complexes with nM to pM affinities.[15,36,53] Importantly, several of these newly formed species have redox potentials that now allow Cu-assisted catalysis of the Fenton reaction.[15,29,36,54]

Since the aberrant labile Cu ion pool is also bound to available ligands, strong chelators are required for effective chelation. However, such strong chelators would also affect the benign non-redox cycling labile Cu^{+} ion pool, like Cu^{+}–glutathione,[12,55] further exacerbating the pathophysiological condition. A novel approach to overcome this challenge is to develop chelators that target the Cu^{2+} labile pool. This pool is mostly non-existent inside cells during physiological conditions,[55] but would be generated as a result of redox cycling during Fenton reaction catalysed by the aberrant Cu ion pool (Fig. 1B and C). Such a chelator would also be expected to protect against Cu^{2+} liberated during protein mis-metallation under oxidative stress conditions.[13,52] Therefore, we set forth to develop cell-permeable chelators that would be able to specifically bind Cu^{2+} over Cu^{+}. Such chelators would not only serve as scaffolds for the development of therapeutics but would also act as strategic chemical tools for elucidating Cu ion homeostasis.

Achieving Cu^{2+} selective chelation against this backdrop would also necessitate the removal of aberrant labile Cu^{2+} without affecting the labile pools of other biological metal ions. The concentration of the labile pools of metal ions like Ca^{2+}, Mn^{2+}, Zn^{2+} and Fe^{2+} range from mM to nM levels.[46,56] Since the ionic radii of divalent transition metal ions fall within 0.7–0.8 Å and all of these metal ions can bind to N and O donor atom containing ligands, designing a selective chelator with a Cu^{2+} binding affinity that is several orders of magnitude higher compared to other metal ions is a significant coordination chemistry challenge.

We have designed a modular synthetic strategy and developed mixed N- and O-donor atom containing Cu^{2+} selective chelators (Scheme 1). The binding constants of the novel chelators toward Cu^{2+} are 10^{8} times higher than that for other biologically relevant metal ions including Cu^{+}. Notably, the binding affinities of the chelators for other divalent metal ions

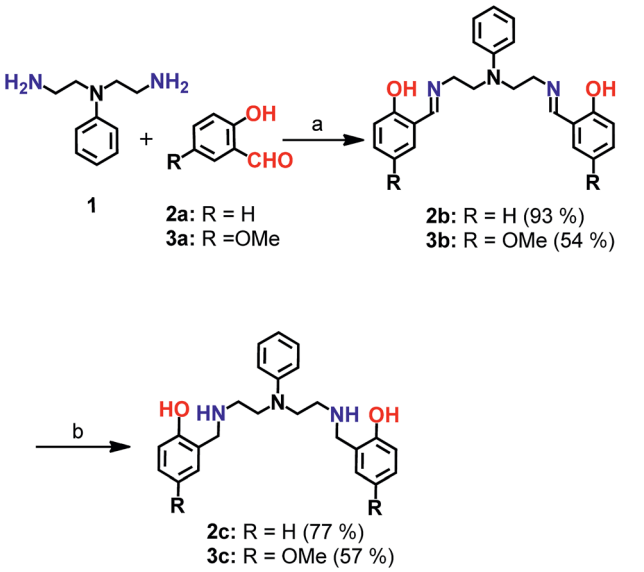

Scheme 1 Synthesis of chelators **2c** and **3c**. [a]Reagents and conditions: (a) sodium acetate buffer, pH 4.5 and methanol, 100 °C; (b) sodium borohydride in dry methanol, 0 °C.

are below the concentrations of their respective labile pools[46,56] and the chelators do not remove protein bound Cu^{2+}. The chelators are cell-permeable and do not affect cell-viability under applied concentrations. These novel molecules suppress Cu^{2+} triggered oxidative stress both in live cells and *in vivo*. Importantly, the chelators were also able to suppress Cu-induced oxidative stress in Menkes disease model Atp7a$^{-/-}$ cells[57] which have endogenously high levels of Cu ions. Hence, our ligands stand out not only in affording exquisite selectivity for Cu^{2+} but also for their applicability to biological systems which we have proven all the way from in cell disease models to a live multicellular vertebrate system.

2. Results and discussion

Chelator synthesis and stability in physiological buffer

Mixed N- and O-donor atom containing ligands were synthesized *via* a modular strategy as shown in Scheme 1. The basic design criterion was to keep the number of synthetic steps minimal. Further, S-donor atoms were avoided to introduce selectivity for Cu^{2+} over Cu^{+}. The precursors **2b**[58] and **3b** were synthesized in a single step by a Schiff base condensation reaction between the amine **1** and either aldehyde **2a** or **3a** (Scheme 1). Compounds **2b** and **3b** were obtained in 93% and 54% yields, respectively. An advantage of this strategy is that the substituent on the aromatic aldehyde could be varied to generate ligands with potentially different metal ion binding affinities. Compounds **2b** and **3b** were reduced in the presence of sodium borohydride. The reduced novel ligands **2c** and **3c** were obtained in 77% and 57% yields respectively starting from **2b** and **3b** (Scheme 1, Fig. S1 and S2†).

Since the chelators would be finally applied in living cells and biological systems, stability in aqueous media was an important criterion.[59] We, therefore, assessed the stability of the molecules over time, using LC/ESI-MS. Both compounds **2c** and **3c** were stable in aqueous buffer as well as in cell-culture medium for over 12 h as shown in Fig. S3.†

Ligands 2c and 3c bind Cu^{2+} ions

The molecules **2c** and **3c** were taken forward for studying Cu^{2+} chelation properties. Absorption titrations for both ligands were performed in the presence of Cu^{2+} ions in aqueous buffer. The absorption spectrum of compound **2c** showed peaks at 247 nm, 277 nm, and a shoulder at 301 nm (Fig. S4†). For compound **3c**, peaks were observed at 247 nm and 295 nm (Fig. S4†).

A distinct new band was observed for both compounds **2c** and **3c** in the presence of Cu^{2+} at 420 nm (ε, 736 M^{-1} cm^{-1}) and 450 nm (ε, 832 M^{-1} cm^{-1}), respectively (Fig. 2a and b, Table S2†). Upon titrating Cu^{2+} to both ligands, the new bands at 420 nm and 450 nm showed increase in intensity with a sharp transition and saturation at 2 equivalents of ligand relative to Cu^{2+} ions (Fig. 2a and b, inset). Other spectral changes were also observed upon Cu^{2+} addition to both ligands. For example, an increase in the intensity of the 275 nm peak was observed for ligand **2c**. Further, the 247 nm peak shifted to 237 nm with concomitant intensity increase (Fig. 2a). Compound **3c** afforded an increase in intensity for both the 247 nm and 295 nm peaks (Fig. 2b). A visible color change was observed from colorless to greenish upon Cu^{2+} addition to both ligands (Fig. S5†). Closer inspection of the absorption spectrum revealed new bands at 623 nm (ε, 173 M^{-1} cm^{-1}) and 626 nm (ε, 275 M^{-1} cm^{-1}), respectively for **2c** and **3c**, which explain the observed color change (Fig. 2c and inset, Table S2†).

Area normalized absorption spectra for Cu^{2+} titration into both ligands showed isosbestic points indicating the presence of distinct Cu^{2+} complexes (Fig. 2d and S6†). The stoichiometry of the complexes was confirmed to be 1 : 2 Cu^{2+} : ligand by the method of continuous variation from Job's plots (Fig. 2e and S7†). The formation of 1 : 2 Cu^{2+} : ligand complexes was further confirmed by ESI/MS analysis (Fig. S8 and S9†). The sharp transitions in absorption titrations (Fig. 2a and b, inset) and Job's plots for **2c** and **3c** with Cu^{2+} (Fig. 2e and S7†) indicated the formation of Cu^{2+} complexes with high binding affinity toward the metal ion. We, therefore, proceeded to determine the stability constants of the ligands with Cu^{2+}. Since, the absorption titrations for both **2c** and **3c** indicated sharp transitions we determined the lower limits for the Cu^{2+} conditional stability constants (β) by simulating binding curves using a 1 : 2 metal : ligand binding model (see ESI†). As shown in Fig. 2f, the data for the titration of Cu^{2+} to **2c** fitted to simulated curves generated by considering log β values ≥12. Similarly, the log β value for Cu^{2+} binding to **3c** was determined to be ≥13 (Fig. S10†).

We also performed electron paramagnetic resonance (EPR) spectroscopy of the Cu^{2+}–**2c** complex in order to obtain insight into its coordination geometry (Fig. S21†). The spin Hamiltonian parameters obtained by simulating the experimental spectrum of the Cu^{2+}–**2c** complex indicate that the Cu^{2+} ion has a tetragonal geometry (pseudo-square planar; $g_{\|} = 2.2220$;

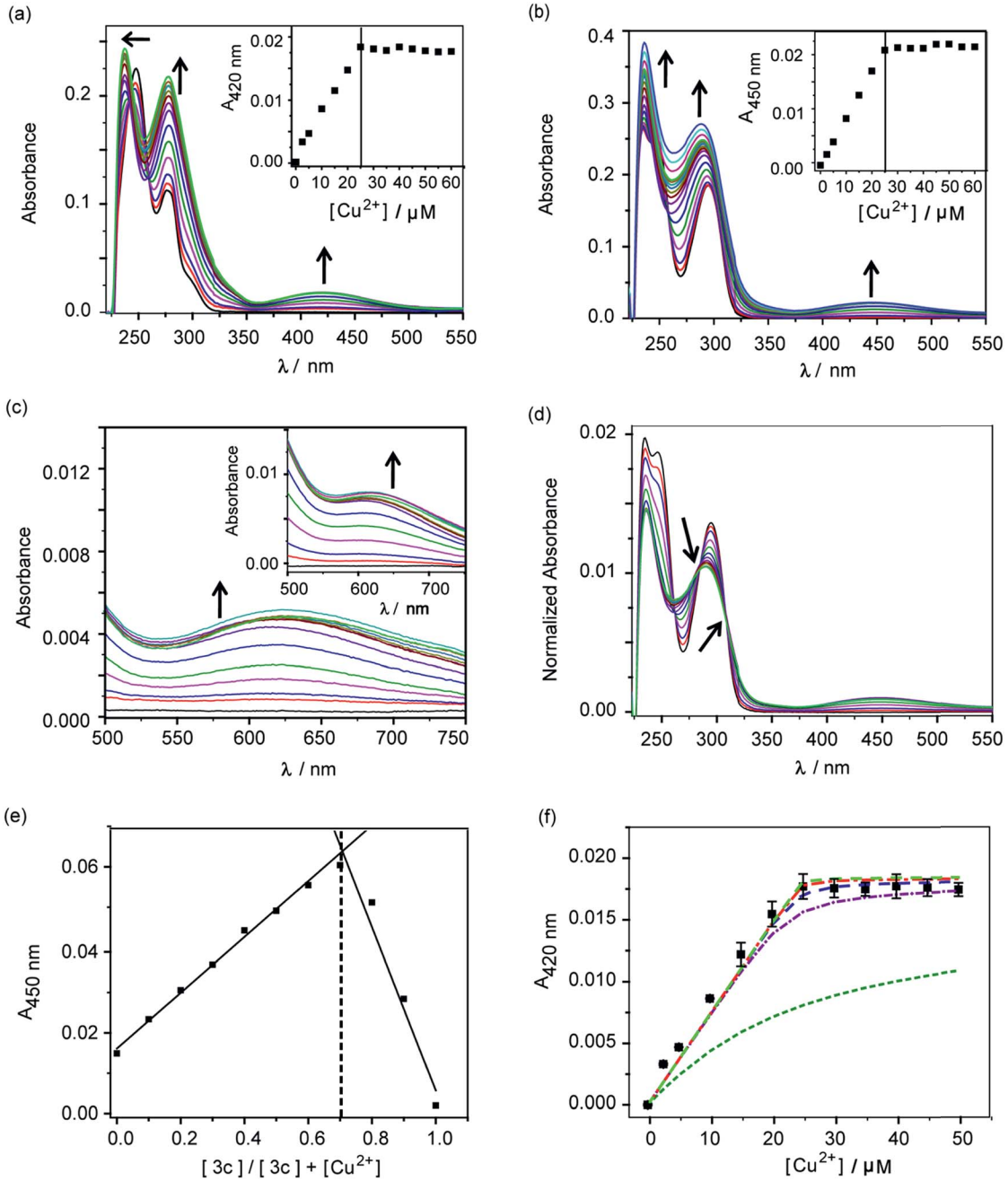

Fig. 2 Absorbance response of ligands **2c** and **3c** with Cu^{2+}. (a) Ultraviolet (UV)-visible titration of **2c** (50 μM) with $CuCl_2$ (0–60 μM) in buffer. Black arrows indicate spectral changes upon addition of Cu^{2+}. The inset shows the plot of absorbance at 420 nm *versus* concentration of Cu^{2+}. (b) UV-visible titration of **3c** (50 μM) with $CuCl_2$ (0–60 μM) in buffer. Black arrows indicate spectral changes upon addition of Cu^{2+}. The inset shows the plot of absorbance at 450 nm *versus* concentration of Cu^{2+}. (c) Visible-near infra-red (NIR) absorbance spectra for titration of **2c** with Cu^{2+}. The inset shows visible-NIR absorbance spectra for titration of **3c** with Cu^{2+}. (d) Area normalized absorbance spectra representing titration of $CuCl_2$ to **3c**. Black arrows indicate isosbestic points. (e) Job's plot depicting absorbance *versus* mole fraction for the Cu^{2+}–**3c** system. (f) Absorption binding plot for titration of Cu^{2+} to **2c** (50 μM, black squares) with simulated fits (fitted to equation: conditional stability constant $\beta = [ML_2]/[M][L]^2$), using log β as 9 (green dashed line), 11 (purple dashed line), 12 (blue dashed line), 13 (red dashed line), 14 (light green dashed line). Buffer used 20 mM HEPES (100 mM NaCl, pH 7.0).

$g_\perp = 2.0502$). The value of $g_\parallel/A_{zz}$ is 120.6 cm. This value is used to assess the degree of geometric distortion and values between 105–135 cm are typical of Cu^{2+} complexes with tetragonal (square planar) geometry.[60] Further, the EPR data indicate that neither un-complexed Cu^{2+} ions nor other Cu^{2+} complexes like di-nuclear Cu^{2+} species are present.

Computed structures of the Cu^{2+} complexes

The UV-visible-NIR titration experiments indicate that **2c** and **3c** coordinate to Cu^{2+} in 1 : 2 Cu^{2+} : ligand stoichiometry. The isosbestic points suggest that the 1 : 2 complexes have a higher stability than the corresponding 1 : 1 complexes (Fig. 2d and

S6†). The UV-visible-NIR spectra of the two complexes indicate that phenolate donors are coordinated to Cu^{2+}, when compared to other ligand systems exhibiting Cu^{2+}–phenolate coordination.[61,62] The electronic transitions at 420 nm (ε, 736 M^{-1} cm^{-1}) and 450 nm (ε, 832 M^{-1} cm^{-1}), respectively, can be assigned to phenolate-based charge-transfer (CT) transitions, while those with significantly lower intensity at 623 nm (ε, 173 M^{-1} cm^{-1}), and 626 nm (ε, 275 M^{-1} cm^{-1}) respectively, are due to d–d transitions. The EPR data indicate the formation of a tetragonal (pseudo square-planar) complex. Taken together the UV-visible-NIR titration and the EPR data indicate the formation of a 1 : 2 Cu^{2+} : ligand complex with a pseudo-square-planar geometry, where two N-and phenolate O-donor atoms each are coordinated to the central metal ion.

In order to obtain further information about the coordination geometries and explore reasons for the formation of 1 : 2 Cu^{2+} : ligand complexes, we used computational methods to predict the corresponding structures. The two ligands **2c** and **3c** are potentially penta-dentate and an important question to answer is: why do the ligands only use either two or three donor atoms each to coordinate to Cu^{2+}? Since ligand-imposed steric strain seems to be a major reason, force field calculations are an ideal approach to get possible answers to this question.

In order to obtain strain energies for comparison between different structures, we have optimized possible 1 : 1 complexes with **2c** as an *O*,*N* bidentate (1^2), an *O*,*N*,*N* (2^3,3^3) or *N*,*N*,*N* tridentate (4^3), an *O*,*N*,*N*,*O* (5^4) or an *O*,*N*,*N*,*N* tetradentate (6^4) and a pentadentate ligand (7^5; not all possible isomers were considered, for details see Fig. S34†). We have used the well-established MOMEC program and force field for the calculations.[63–67] Additional parameters involving Cu^{2+}–$O_{phenolate}$ bonding were obtained from known structures[61,62] (see ESI, Table S5†). All Cu^{2+} centers were computed as Jahn–Teller elongated hexa-coordinate geometries with water molecules completing the coordination spheres, and the conformational space was evaluated deterministically. Details of the computational analysis have been included in the ESI.†

The structure with **2c** coordinated as an *O*,*N* bidentate ligand (1^2) afforded the lowest strain energy. The only other structures that might compete in terms of steric strain were those with **2c** as a tridentate or tetradentate ligand involving amino-salicylate donor groups (2^3 and 5^4), and these structures were 15 and 11 kJ mol^{-1} higher in energy, respectively than the 1^2 structure (Fig. S34 and Table S6†). However, these structures involve relatively flexible 8-membered chelate rings and therefore are entropically disfavored. Due to severe van der Waals repulsion by the phenyl substituent of the tertiary amine donor, all other isomers are destabilized by an additional 15–20 kJ mol^{-1}. The optimized structures of the lowest energy 1 : 1 and 1 : 2 Cu^{2+} : **2c** complexes are presented in Fig. 3 and ESI Video.† Hence, we infer that these ligands coordinate to Cu^{2+} in a bidentate mode with high 1 : 2 metal : ligand Cu^{2+} binding constants. Although we cannot completely rule out the possibility of the formation of minor ternary complexes with available ligands from the media, we note that the structure of the 1 : 2 Cu^{2+} : **2c** complex is in agreement with the UV-visible-NIR spectra, the spectrophotometric titration, the ESI-MS spectra, and the EPR spectrum.

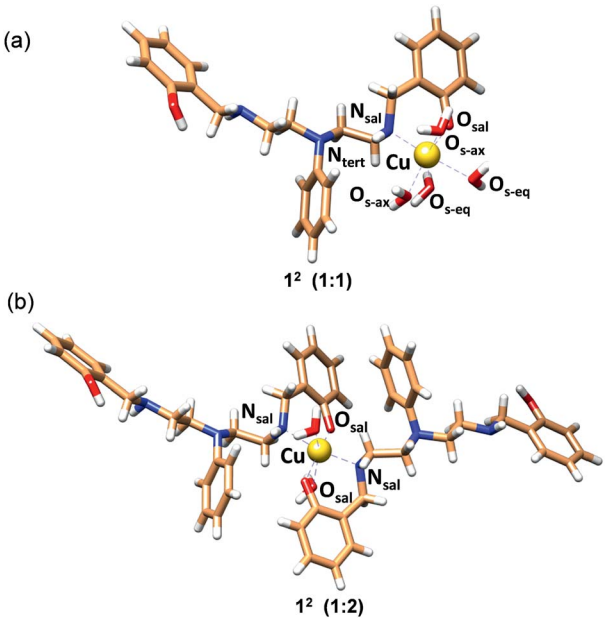

Fig. 3 MOMEC optimized structures for (a) $[Cu^{2+}(\mathbf{2c})(OH_2)_4]$ (1^2; 1 : 1) and (b) $[Cu^{2+}(\mathbf{2c})_2(OH_2)_2]$ (1^2; 1 : 2) complexes. Ligand **2c** is in the phenolate form. In the structures, carbon, nitrogen, oxygen and hydrogen atoms are represented in light brown, blue, red and white colors, respectively. Copper ions are represented in gold.

Competition experiment of 2c and 3c with a high affinity Cu^{2+} chelator and protein-bound Cu^{2+}

We next performed a control experiment in which ethylenediamine tetra-acetic acid (EDTA) was titrated into a solution containing 1 : 2 Cu^{2+} : ligand **3c**. The absorption band at 450 nm decreased with increasing concentrations of EDTA and the band completely attenuated at ~0.75 equivalent of EDTA (Fig. S11†). The Cu^{2+}–EDTA (1 : 1) complex has a log β of 15.8.[68] This control experiment indicated that the ligands would not be able to chelate out Cu^{2+} from essential enzymes that have Cu^{2+} binding affinities in the aM–fM regime.[50] To further confirm that the chelators will not affect enzyme bound copper, we titrated the chelators to Cu^{2+}–azurin complex which has a Cu^{2+} dissociation constant of 25 fM.[69] Cu^{2+}–azurin complex has a characteristic absorption peak at 628 nm due to cysteine–Cu^{2+} charge-transfer.[70] The absorption of the peak remained unaffected even upon addition of upto 12 equivalents of the chelators **2c** and **3c** (Fig. S12†). Therefore, the chelators **2c** and **3c** will be able to remove excess labile copper without affecting enzyme bound copper.

Selectivity of the chelators toward Cu^{2+}

Encouraged by the Cu^{2+} binding data we evaluated the conditional stability constants of **2c** and **3c** toward other biologically relevant metal ions that can bind to ligands with mixed N- and O-donor atoms. Absorption titrations for both ligands were performed in the presence of Cu^{+}, Ca^{2+}, Fe^{3+}, Fe^{2+}, Ni^{2+}, Zn^{2+}, Mn^{2+} and Co^{2+} metal ions (Fig. S13–S20†). The titration curves indicated weak binding and the data could be fitted to a 1 : 1 binding model. The conditional stability constants ranged

between log β values of 2.53 to 4.48 (Table 1) indicating that the stability constants of the ligands toward Cu^{2+} were at least 10^8 times higher than the stability constants toward Cu^{+}, Ca^{2+}, Zn^{2+}, and other transition metal ions. The binding data indicated that **2c** and **3c** were indeed highly selective Cu^{2+} chelators (Table 1).

None of the existing commercial Cu^{2+} chelators that are used for either therapy of Cu-overload diseases or for mechanistic studies in elucidating Cu regulation afford such distinct selectivity toward Cu^{2+} (Table S3†).[27,71] In fact, when we compared the reported binding constants of these commercial ligands for Cu^{2+} *versus* other metal ions we found that most of them bind more strongly to Fe^{3+} and also have very high affinities toward Zn^{2+} and Ni^{2+}.[27,71] We also compared our chelators to the few other previously reported reduced salen chelators[23,68] (Table S4†). Unlike our chelators the metal binding constants of these reduced salen chelators for most biologically relevant metal ions had not been reported. We found that our ligands stood out in their selectivity toward Cu^{2+} relative to the majority of this group as well.

Since the spectroscopic characterization and computed structures of the Cu^{2+}–**2c** complex indicate that only half of the ligand comprising a phenolate O atom and the secondary N atom coordinate to the metal ion we investigated if a minimal control binding unit, 2-((benzylamino)methyl)phenol, would be sufficient to explain the observed selectivity. Absorption titration data of Cu^{2+} to the control molecule (performed under same experimental conditions as **2c** and **3c**, Fig. S22†) indicated that the ligand can bind to Cu^{2+} ions in 1 : 2 Cu^{2+} : ligand stoichiometry with a log β value of 7.0. However, interestingly, the ligand did not afford a change in its absorption spectrum in the presence of other essential metal ions under identical experimental conditions, suggesting that the stability constants of the ligand toward other metal ions were very low (Fig. S23†). This data indicates that the control molecule, although a weaker Cu^{2+} binder (log β 7.0) compared to **2c** and **3c** (log $\beta \geq$ 12), retains its selectivity for Cu^{2+} binding. This result suggests that the other half of the molecules **2c** and **3c** would be important in pre-orienting the binding unit for Cu^{2+} coordination thereby increasing the binding affinity. Further, the computational studies show that the steric strain provided by the central *N*-phenyl moiety drives the binding toward a bidentate mode and disfavors the use of other donor atoms in the ligand. This is a key feature that leads to Cu^{2+} selectivity since the resultant pseudo square-planar (tetragonal) geometry adopted by the Cu^{2+} complex is a highly preferred ligand orientation for d^9 Cu^{2+} systems when compared to other metal ions. We next proceeded to test the ability of our chelators to alleviate Cu-induced oxidative stress.

Table 1 Conditional stability constant (log β) for the chelators with different metal ions

Compound	Cu^{2+}	Cu^{+}	Mn^{2+}	Co^{2+}	Zn^{2+}	Ca^{2+}	Fe^{2+}	Fe^{3+}	Ni^{2+}
2c	≥12	4.19	n.b[a]	3.97	3.93	n.b[a]	3.63	3.39	2.53
3c	≥13	4.48	4.20	n.b[a]	3.90	n.b[a]	4.05	3.89	3.10

[a] No binding was detected. Conditional stability constant, $\beta_{1n} = [ML_n]/[M][L]^n$; $n = 2$ for Cu^{2+} and $n = 1$ for other metal ions. All the absorbance measurements were carried out in 20 mM HEPES buffer (100 mM NaCl, pH 7.0).

Chelators reduce Cu ion catalyzed hydroxyl radical production *in vitro*

First, an *in vitro* deoxyribose-based assay[72] was performed to test whether the chelators could suppress Cu ion catalyzed formation of hydroxyl radicals. In this assay, deoxyribose reacts with *in situ* generated hydroxyl radicals to produce malondialdehyde. Malondialdehyde reacts with thiobarbituric acid to produce a pink chromophore with absorbance maxima at 532 nm (Fig. S24†). If a ligand is able to chelate Cu^{2+} from the reaction mixture then the production of the chromophore would be reduced. Importantly, Cu^{2+} chelation would reduce the production of hydroxyl radicals provided the metal complex does not promote further Fenton reaction. The absorbance of the chromophore at 532 nm is therefore used as a readout for Cu ion catalyzed production of hydroxyl radicals.

Both ligands **2c** and **3c** suppressed the production of hydroxyl radicals as seen from the reduction of the absorbance at 532 nm (Fig. 4). Desferrioxamine mesylate (DFO) was used as a positive control since DFO is a known chelator for redox active metal ions like iron and copper. A related ligand desferrioxamine B which does not have the mesylate groups has a stability constant log β value of 14.1 for a 1 : 1 Cu^{2+} : ligand complex.[71] The plots for absorbance at 532 nm *versus* chelator concentration for ligands **2c** and **3c** followed a similar trend as that of DFO with greater than 90% reduction in absorbance at concentrations above 50 μM (Fig. 4). On the other hand, salicyaldehyde, a weaker chelator (log β for Cu^{2+} 7.4)[71] only partially reduced the formation of hydroxyl radicals (Fig. 4). The deoxyribose assay clearly indicated that the ligands **2c** and **3c** would be able to chelate Cu^{2+} and suppress Cu ion induced hydroxyl

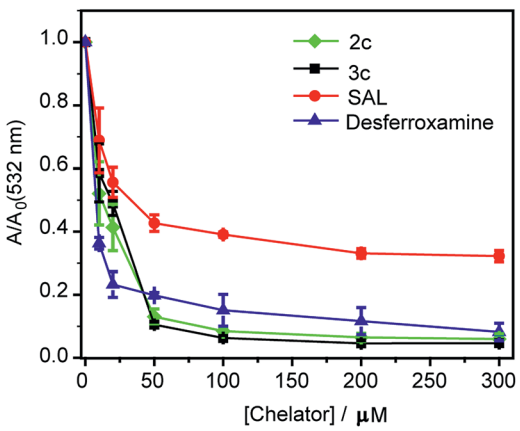

Fig. 4 Effect of chelators **2c** and **3c** on deoxyribose degradation *via* Cu ion mediated hydroxyl radical formation. Salicylaldehyde (SAL) and desferroxamine mesylate (DFO) were used as controls. Ratio of values of absorbance in the presence of chelator (*A*) *versus* absorbance in the absence of chelator (A_o) <1 signify protection against hydroxyl radical mediated deoxyribose degradation. Conditions: $CuSO_4$ (10 μM), 2-deoxyribose (15 mM), H_2O_2 (100 μM), ascorbic acid (2 mM), at pH 7.4 in phosphate buffer.

radical formation. Importantly, unlike chelators such as DFO which have extremely high binding affinities for most metal ions,[71,73] our chelators are highly selective for Cu^{2+}. The *in vitro* assay also indicated that the Cu^{2+} complexes of **2c** and **3c** would not promote further Fenton chemistry. This is an important criterion for Cu chelation targeted toward assuaging Cu-induced oxidative stress since there are multiple examples of chelators that can bind to Cu^{2+} and promote the production of hydroxyl radicals.[52,74–77] Hence, our chelators can be potentially useful for treating Cu ion overload associated disorders.

Chelators remove Cu ions from Cu^{2+} exposed living cells

As a first step toward evaluating the chelators in living systems, we wanted to test whether the chelators could remove Cu ions from Cu^{2+} overloaded cells. Phen Green FL diacetate is a cell permeable fluorescent dye that is quenched in the presence of Cu ions, and has been used effectively to image intracellular Cu ions in Cu^{2+} overloaded biological systems.[78–80] Human embryonic kidney cells (HEK293T) were used for the experiments. Cells were incubated with Phen Green FL and imaged in a confocal microscope. In comparison to control untreated cells the Cu^{2+}-treated cells showed a significant decrease in fluorescence intensity (Fig. 5a and c, $***p \leq 0.001$). When the Cu^{2+}-treated cells were incubated with the chelators **2c** and **3c** for 30 min the Phen Green fluorescence intensities afforded significant recovery and were similar to the Cu^{2+} untreated controls (Fig. 5b and c). The recovery of Phen Green fluorescence upon chelator treatment in Cu^{2+} overloaded cells along with the distinct Cu^{2+} selectivity of our chelators indicate that these chelators will be able to efficiently remove Cu^{2+} ions from cells under oxidative stress conditions.

Chelators suppress Cu induced oxidative stress in living cells

Our *in vitro* data had shown that the chelators could attenuate Cu induced production of hydroxyl radicals which is a major pathway by which Cu ions cause oxidative damage. We have also validated that our chelators would be able to remove Cu^{2+} ions from live cells. The next key step was to test the ability of the chelators to alleviate Cu^{2+} induced oxidative stress in living cells. HEK293T cells were incubated with Cu^{2+} and the level of reactive oxygen species (ROS) in the cells was monitored using CellROX® Deep Red[81] which emits in the red (λ_{ex}: 633 nm, λ_{em}: 641–700 nm) upon oxidation with ROS (Fig. 6 and S25†). Fig. 6 depicts confocal images of live HEK293T cells. The basal level of ROS in cells was determined by using control cells that had not been treated with Cu^{2+}. Addition of the chelators to cells did not cause any increase in the emission intensity of CellROX indicating that the chelators alone did not induce any oxidative stress (Fig. 6). Cu^{2+} treated cells induced a significant increase in ROS over control untreated cells ($****p \leq 0.0001$, Fig. 6). Both $CuCl_2$ (Fig. 6) and $CuSO_4$ (Fig. S25†) showed similar CellROX responses indicating that the oxidative stress was due to Cu^{2+}, rather than the anion. Finally, when the Cu^{2+} treated cells were incubated with the chelators a significant decrease in the CellROX emission intensity was observed indicating that both ligands **2c** and **3c** were able to rescue the cells from Cu^{2+} induced oxidative stress conditions

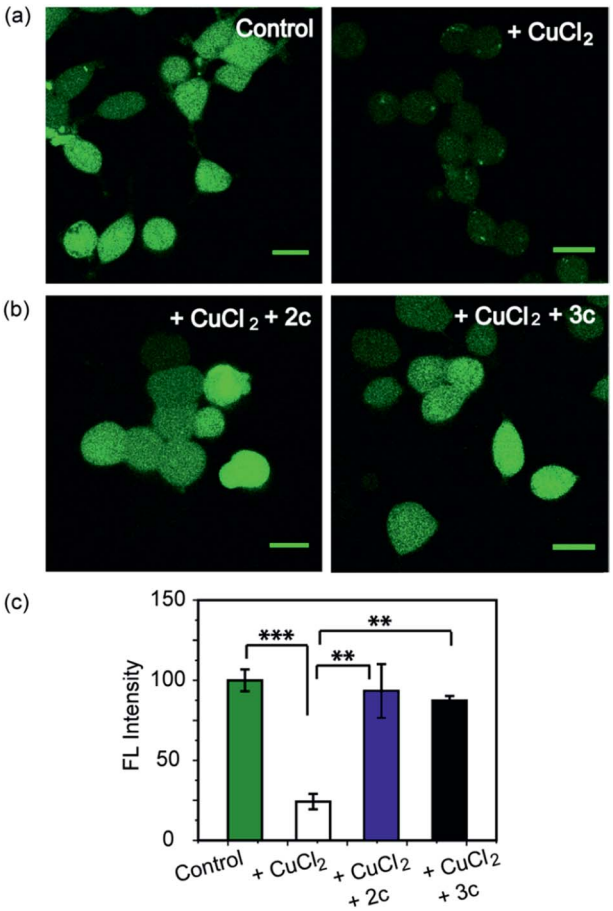

Fig. 5 Confocal fluorescence images of live HEK293T cells to show the effect of Cu^{2+} chelators using a Cu ion responsive dye Phen Green FL. All cells were incubated with Phen Green FL dye (5 μM) initially for 30 min before any further treatments. (a) Left to right: control cells; cells treated with $CuCl_2$ (20 μM) for 30 min. (b) Left to right: cells treated with $CuCl_2$ (20 μM) for 30 min followed by **2c** (80 μM) for 30 min; $CuCl_2$ (20 μM) for 30 min followed by **3c** (80 μM) for 30 min. Cells were washed three times with PBS buffer after each addition and then imaged ($\lambda_{ex/em}$: 488/498–600 nm). Fluorescence intensity analyses of confocal images were carried out by using ImageJ software. (c) Bar plots represent the intensity analyses results. Intensity data were normalized to intensity of control untreated cells. Error bars denote SEM, $n = 3$. Statistical analyses were performed using an unpaired, two-tailed Student's *t*-test ($**p \leq 0.01$, $***p \leq 0.001$). Images were acquired using a 40× objective; scale bar: 20 μm.

(Fig. 6 and S25†). Moreover, pre-treating the cells with the chelators prior to Cu^{2+} incubation also protected the cells from Cu-induced oxidative stress (Fig. S26†).

Fe^{2+} ions also catalyse Fenton reaction. However, our chelators being Cu^{2+} specific should not alleviate Fe-induced oxidative stress. A control experiment in the presence of Phen Green which also responds to Fe^{2+} indicated that the chelators could not remove Fe ions from cells treated with an Fe^{2+} salt (Fig. S27†). Further, CellROX fluorescence also increased in cells incubated with Fe^{2+} indicating increased oxidative stress. However, the chelators could not reduce CellROX fluorescence (Fig. S28†) confirming the selectivity of our chelators toward Cu^{2+} in live cells.

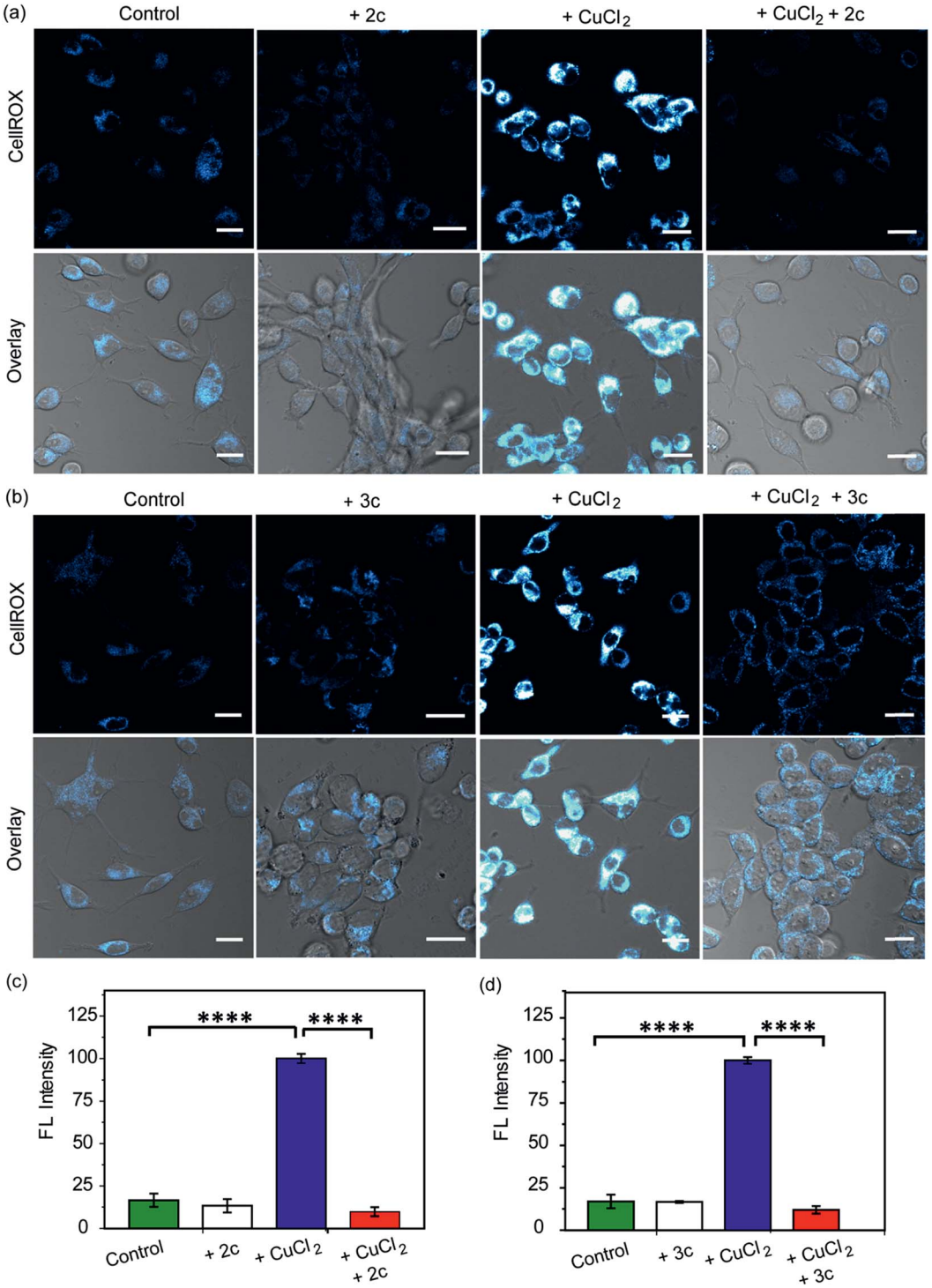

Fig. 6 Confocal fluorescence images of live HEK293T cells in presence of chelators and a ROS sensitive dye. (a) Left to right: control cells; cells treated with chelator **2c** (40 μM) for 30 min; with $CuCl_2$ (20 μM) for 30 min; with $CuCl_2$ (20 μM) for 30 min followed by **2c** (40 μM) for 30 min. (b) Left to right: control cells; cells treated with **3c** (40 μM) for 30 min; $CuCl_2$ (20 μM) for 30 min; $CuCl_2$ (20 μM) for 30 min followed by **3c** (40 μM) for 30 min. Cells were stained with CellROX (5 μM) for 30 min at the final step before imaging. ($\lambda_{ex/em}$: 633/641–700 nm). Cells were washed three times with PBS buffer after each addition and then imaged. Lower panels of (a) and (b) shows bright field images of cells overlaid with confocal images. Fluorescence intensity analyses of confocal images were carried out by using ImageJ software. Bar plots represent the intensity analyses results for (c) chelator **2c** and (d) chelator **3c**. Intensity data were normalized to intensity of $CuCl_2$ treated cells. Error bars denote SEM, $n = 3$. Statistical analyses were performed using an unpaired, two-tailed Student's *t*-test (****$p \leq 0.0001$). Images were acquired using a 40× objective; scale bar: 20 μm.

As a positive control, D-penicillamine (D-Pen)[27,82] a cell-permeable non-selective Cu^{2+} chelator (Table S3†) also suppressed Cu^{2+} induced oxidative stress to a similar extent as chelators **2c** and **3c** (Fig. 6a–d and S29a, b†). However, our chelators are highly selective toward Cu^{2+} and hence have a significant advantage over other non-specific Cu^{2+} chelators. In order to further confirm that the chelators **2c** and **3c** indeed reduce Cu^{2+}-induced oxidative stress *via* Cu^{2+} chelation and not *via* the removal of ROS through reactions with the phenolic moieties in the chelators,[83,84] we performed an additional control experiment by monitoring the effect of the chelators on lipopolysaccharide induced oxidative stress. Lipopolysaccharides generate ROS *via* the activation of toll-like receptors which in turn activate NADPH oxidase leading to oxidative stress.[85,86] Both chelators **2c** and **3c** had no effect on LPS induced oxidative stress in live cells demonstrating that the chelators function *via* Cu^{2+} chelation in alleviating Cu-induced oxidative stress (Fig. S29c and d†).

Further, we simultaneously imaged Cu ions and ROS in live cells to firstly show that regions of high ROS in Cu-overloaded cells colocalize with Cu ions; and secondly to show that the chelators can access these regions, chelate out Cu^{2+}, and efficiently reduce the ROS burden. Phen Green FL and CellROX Deep Red were used to image Cu ions and ROS respectively. Cu^{2+} untreated cells showed high Phen Green intensity and low CellROX intensity indicating low Cu^{2+} and low ROS levels, respectively (Fig. 7A, B and C, a panels). Cells treated with Cu^{2+} showed low Phen Green intensity due to quenching of the Phen

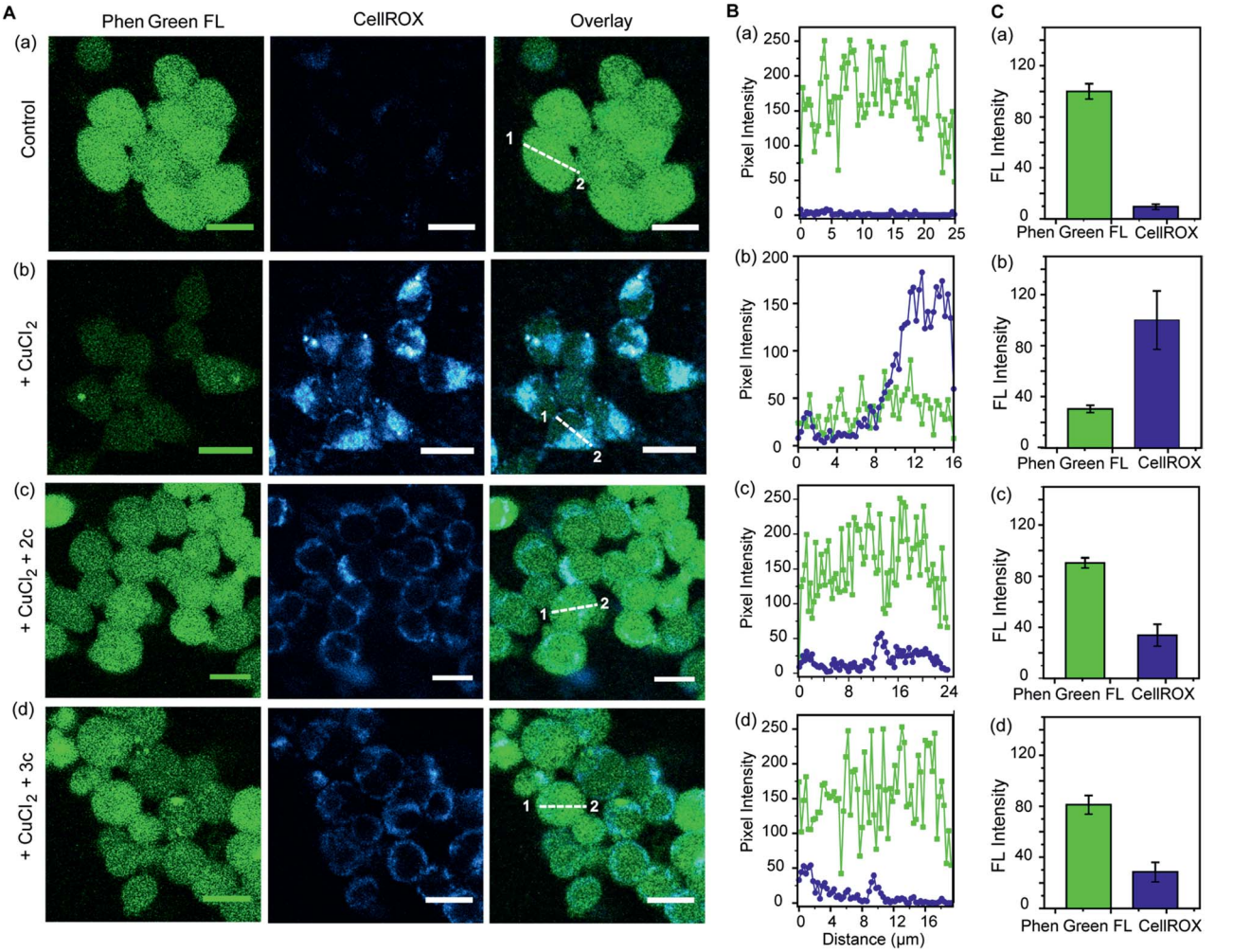

Fig. 7 Simultaneous imaging of copper levels and oxidative stress in live HEK293T cells in the presence and absence of chelators **2c** and **3c**. Phen Green FL was used to image Cu ions and CellROX was used to image ROS. (A) Top to bottom (a–d): confocal images of control untreated cells; cells treated with $CuCl_2$ (20 μM) for 30 min; cells treated with $CuCl_2$ (20 μM) for 30 min followed by **2c** (80 μM) for 30 min; cells treated with $CuCl_2$ (20 μM) for 30 min followed by **3c** (80 μM) for 30 min. All cells were incubated with Phen Green FL (5 μM) for 30 min prior to any other treatment ($\lambda_{ex/em}$: 488/498–600 nm) and incubated with CellROX (5 μM) for 30 min at the final step before imaging ($\lambda_{ex/em}$: 633/641–700 nm). Cells were washed three times with PBS buffer after each addition and then imaged. Number of washings was identical for all experiments. Left to right: HEK293T cells showing Phen Green FL emission, CellROX emission, and overlaid confocal images. (B) The white lines in the overlaid images were used to calculate the fluorescence intensity of Phen Green FL (green) and CellROX (blue) in the line scan along the direction of 1 to 2. (C) Bar plots represent the intensity analyses results for panel (A, a–d). Intensity data were normalized to intensity of control untreated or $CuCl_2$ treated cells. Error bars denote SEM, $n = 3$. Images were acquired using a 40× objective; scale bar: 20 μm.

Green fluorescence by Cu ions throughout the cells (Fig. 7A, B and C, b panels). CellROX intensity was high in the cytoplasm indicating oxidative stress conditions (Fig. 7A, B and C, b panels). Upon treatment with the chelators, the Phen Green intensity recovered with a simultaneous decrease in the CellROX intensity from the cytoplasm indicating that the chelators can distinctly reduce Cu^{2+} induced oxidative stress in live cells *via* Cu^{2+} chelation (Fig. 7A, B and C, c and d panels).

Finally, we checked whether the chelators would affect cell-viability. More than 93% cells were viable up to 4 h of incubation with 100 μM of the chelators (Fig. S30†). Hence, the chelators would have minimal toxicity when applied up to micro molar levels (Fig. S30†). All of the confocal imaging experiments, intensity analyses of the images, and cell-viability data taken together highlight the efficacy of the novel chelators toward alleviating Cu ion induced oxidative stress conditions and indicate the potential of the chelators toward therapeutic applications. We, therefore, took the chelators a next step forward and tested their applicability in a cellular disease model representing endogenous Cu ion overload.

Effect of chelators on oxidative stress in an Atp7a$^{-/-}$ cell model of Menkes disease

In order to ascertain the efficacy of our Cu^{2+} selective chelators in a disease model of copper overload, we tested the ligands **2c** and **3c** in mouse embryonic fibroblast cells lacking the *Atp7a* gene, which is mutated in Menkes disease (Fig. S31† and 8).[57] ATP7A is a P-type ATPase required for copper export. Loss of ATP7A function causes copper hyper-accumulation,[41,87] and previous ICP-MS studies have shown that the Atp7a$^{-/-}$ mouse embryonic fibroblast cells accumulate 6-fold more copper in the cytoplasm compared to isogenic wildtype cells.[57] Higher Cu levels would induce oxidative stress provided the excess Cu ions are bound to cellular ligands that promote redox cycling leading to Cu ion catalyzed ROS production. Therefore, we decided to check the level of ROS in the Atp7a$^{-/-}$ mouse embryonic fibroblast cells. The Atp7a$^{-/-}$ cells showed significantly higher oxidative stress compared to the wildtype cells (Fig. 8a–d left panels, and Fig. 8e and f). This data implied that the increased endogenous level of Cu ions in the Atp7a$^{-/-}$ cells were capable of promoting oxidative stress. Importantly, both **2c** and **3c** were able to reduce the levels of oxidative stress in the Atp7a$^{-/-}$ cells (Fig. 8a–d right panels, Fig. 8e and f). This data demonstrates the efficacy of **2c** and **3c** against endogenous Cu ion overload induced oxidative stress.

The fact that our chelators reduce oxidative stress *via* Cu^{2+} ion chelation has been established both directly (Fig. 7A–C) and through control experiments in the presence of LPS (Fig. S29c and d†). These results when combined with the data on the Atp7a$^{-/-}$ cells, indicate that Cu ion overload is indeed associated with increased oxidative stress catalyzed by Cu species that can perform redox cycling to generate ROS. Our chelators catch the Cu ions in the +2 oxidation state and generate a chelated species that blocks the redox cycling to alleviate Cu-induced oxidative stress. Hence, we decided to check the efficacy of the chelators in a multicellular, vertebrate model system.

Chelators alleviate oxidative stress *in vivo* in a zebrafish larval model

To evaluate the efficacy of **2c** and **3c** compounds *in vivo*, we investigated their ability to modulate pathways of redox signaling using a zebrafish model. Zebrafish larvae have emerged as a robust vertebrate model system for toxicological studies aimed at understanding the effects and mechanisms underlying oxidative stress.[88–90] Pathways related to redox signaling and lipid metabolism in zebrafish are highly analogous to those in humans.[91,92] According to literature reports zebrafish have an enhanced oxidative stress response.[93–95] One of the major factors responsible for the increased oxidative stress response is the presence of comparatively high levels of unsaturated fatty acids that help fish maintain the fluidity of cell membranes at lower temperatures.[92] The optical transparency of zebrafish larvae make them suitable for optical imaging with ROS sensitive optical probes like CellROX.[81] We, therefore, tested the efficacy of the chelators toward alleviating Cu^{2+} induced oxidative stress in live zebrafish larvae.

3.5 days post fertilization (dpf) wildtype zebrafish larvae were exposed to Cu^{2+} by incubating the larvae in a medium containing copper salts. The larvae treated with copper salts exhibited increased oxidative stress as observed by increased intensity of CellROX. Highest intensities were observed in the tail muscles, gut, lateral fins, and around the eyes of the larvae (Fig. 9a). The swimming motion of zebrafish larvae are well-established where the larvae perform C-start motions during which the tail fin is bent into a C-shape.[96,97] This movement helps the fish propel itself forward and dictates the speed of swimming.[96,97] The C-start movement is an energy-demanding process for the muscles in the tail fin implying high mitochondrial activity in this region. Further, the lateral fins help the fish maintain balance during swimming which is also associated with increased muscle activity in these regions.[98] The gut undergoes spontaneous peristaltic movements starting from 2 dpf. These peristaltic movements are driven by the gut muscles which are controlled by the autonomous nervous system.[99] Finally, the zebrafish larvae actively scan their lateral field of view as they swim to visualize their environment which requires extra-ocular muscles that help in eye movement.[100] In summary, we noted that the anatomical regions that showed increased oxidative stress in the zebrafish larvae upon Cu exposure were regions of high muscle activity and hence would be associated with greater mitochondrial density.[81,101] Since, hydrogen peroxide production increases with increased mitochondrial activity,[102,103] these regions would be more susceptible to metal induced oxidative stress *via* the Fenton pathway in accordance with our observation (although other regions might also accumulate metal ions).

We were pleased to note that the level of oxidative stress in the Cu-treated larvae significantly decreased in the presence of the chelators to levels similar to untreated larvae (Fig. 9b and d). The **2c** and **3c** chelators alone did not induce any oxidative stress in the larvae (Fig. S32†), and their ability to suppress copper-stimulated ROS was similar to D-Pen (Fig. S33†). Control experiments with LPS treated larvae showed that **2c** and **3c**

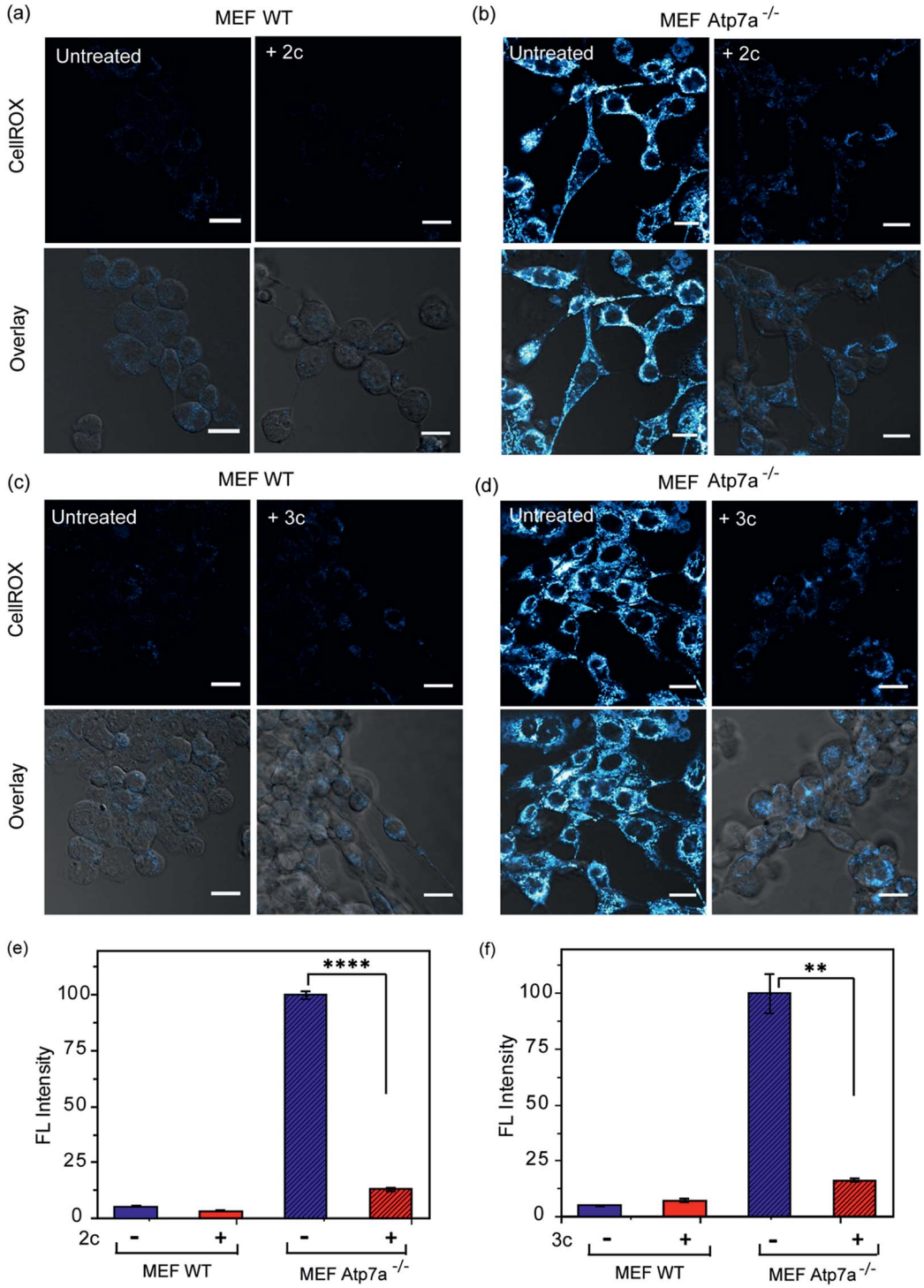

Fig. 8 Confocal fluorescence imaging in mouse embryonic fibroblast wildtype (MEF WT) and mouse embryonic fibroblast *Atp7a* knockout (MEF Atp7a$^{-/-}$) cells in presence of chelators and a ROS sensitive dye. (a) MEF WT cells: left to right, untreated cells; cells treated with chelator **2c** (40 μM) for 60 min. (b) MEF Atp7a$^{-/-}$ cells: left to right, untreated cells; cells treated with chelator **2c** (40 μM) for 60 min. (c) MEF WT cells: left to right, untreated cells; cells treated with chelator **3c** (40 μM) for 60 min. (d) MEF Atp7a$^{-/-}$ cells: left to right, untreated cells; cells treated with chelator **3c** (40 μM) for 60 min. Cells were stained with CellROX (5 μM) for 30 min at the final step before imaging ($\lambda_{ex/em}$: 633/641–700 nm). Cells were washed three times with PBS buffer after each addition and then imaged. Lower panels of (a)–(d) shows bright field images of cells overlaid with confocal images. Fluorescence intensity analyses of confocal images were carried by using ImageJ software. Bar plots represent the intensity analyses of fluorescence images for chelators (e) **2c** and (f) **3c**. Fluorescence intensities were normalized to intensity of MEF Atp7a$^{-/-}$ cells. Error bars denote SEM, $n = 3$. Statistical analyses were performed using an unpaired, two-tailed Student's *t*-test (**$p \leq 0.01$, ****$p \leq 0.0001$). Images were acquired using a 40× objective; scale bar: 20 μm.

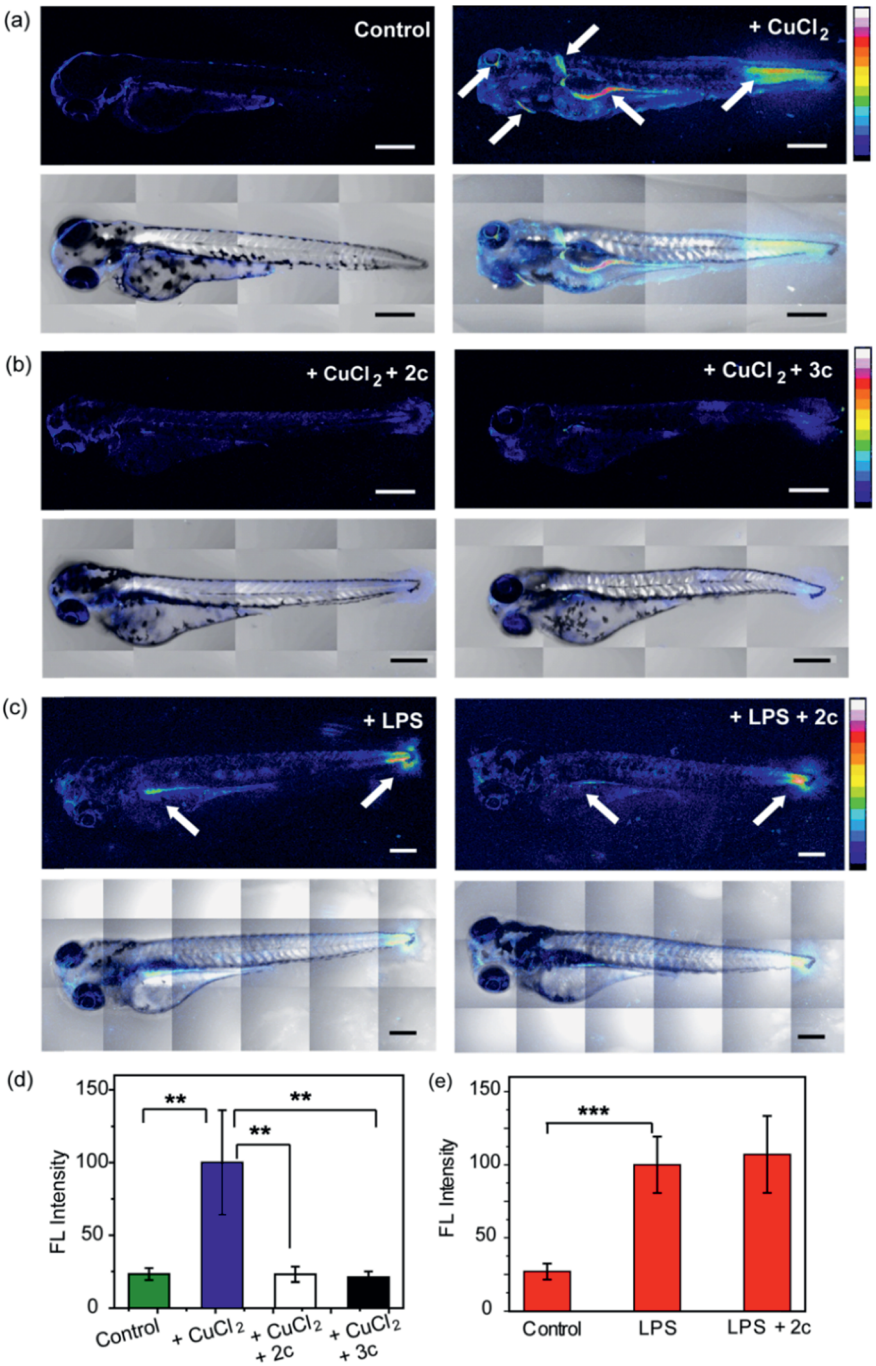

Fig. 9 Confocal fluorescence images depicting the effect of chelators on live 3.5 dpf zebrafish larvae treated with copper salts. (a–c) Upper panels depict Z stacked confocal fluorescence images and lower panels depict bright field images overlaid with Z stacked confocal fluorescence images. (a) Control Cu-untreated larvae (left) and larvae treated with $CuCl_2$ (30 μM) for 30 min (right). (b) Larvae treated with $CuCl_2$ (30 μM) for 30 min followed by **2c** (60 μM) for 30 min (left) and larvae treated with $CuCl_2$ (30 μM) for 30 min followed by **3c** (60 μM) for 30 min (right). (c) Larvae treated with LPS (10 μg mL^{-1}) for 30 min (left) and larvae treated with LPS (10 μg mL^{-1}) for 30 min followed by **2c** (60 μM) for 30 min (right). White arrows indicate regions exhibiting high oxidative stress. Larvae were stained with CellROX (10 μM) for 30 min in the final step before imaging. (d) Bar plots representing average fluorescence intensities obtained from intensity analysis of confocal images of the zebrafish larvae experiments for which representative images are shown in panels (a and b). Intensity data were normalized to intensity of $CuCl_2$ treated larvae. (e) Quantification of fluorescence intensities of confocal images of zebrafish larvae for which representative images are shown in panel (c). Intensity data were normalized to LPS treated larvae. For both panels (d and e) intensity analyses were carried out on Z-stacked confocal images of zebrafish larvae. ImageJ software (NIH, USA) was used for image analysis. For fluorescence quantification, a region of interest (ROI) was created, and fluorescence intensity was measured. The reported fluorescence intensity was determined by averaging the measured intensity of at least fifteen different ROIs from experiments on at least six different zebrafish larvae. Error bars denote SEM, $n = 6$. Statistical analyses were performed using an unpaired, two-tailed Student's t-test (**$p \leq 0.01$, ***$p \leq 0.001$). 20× objective was used for imaging; scale bar: 200 μm.

could not rescue LPS induced oxidative stress (Fig. 9c and e). Therefore ligands **2c** and **3c** suppress Cu ion induced oxidative stress *via* Cu^{2+} chelation in a multicellular, vertebrate organism indicating the *in vivo* applicability of the chelators.

3. Concluding remarks

The regulation of redox active metal ions involves the intricate interplay of multiple proteins and biological ligands and exhibits many shades of subtle homeostatic balance.[56,104] While the concept of chelation therapy has a long history, the appreciation of the balance between the labile and the protein bound pool and the regulatory factors that maintain this balance is very recent.[105] Hence, most chelation therapy based approaches for treating metal-overload disorders are based on chelators that are non-specific.[27] These non-specific chelators are also frequently used for mechanistic studies in unravelling metal ion regulation, leading to equivocal information on metal ion homeostasis.[104,105] The development of selective chelators for a specific oxidation state of a redox-active metal ion remains a significant challenge, but is extremely worthwhile given the wealth of mechanistic information that can be obtained by the judicious use of such chelators and the tremendous potential in minimizing the side-effects associated with chelation therapy.

By analyzing the literature on Cu-induced oxidative stress and Cu ion speciation in cells,[56,105] we realized that chelating out Cu^{2+} ions which would mostly be generated under oxidative stress conditions inside cells would provide access to selective Cu ion chelation without affecting the essential intracellular metal pool. An important criterion was that the chelated Cu^{2+} should not further promote Fenton chemistry. Using our redox-state selective chelation strategy, we have therefore developed novel chelators that exhibit unique Cu^{2+} selectivity and can alleviate metal overload induced oxidative stress both *in vitro* and in live cells. Importantly, we were able to show that the chelators reduce oxidative stress *via* Cu^{2+} chelation rather than by direct ROS scavenging, and were able to suppress ROS production in a disease model of cellular Cu overload. Finally, the chelators were able to reduce Cu-induced oxidative stress in zebrafish larvae indicating their ability to function *in vivo*.

The high selectivity of our chelators for Cu^{2+} over Cu^{+} and other biologically relevant metal ions makes these scaffolds valuable chemical tools for exploring pathways of Cu ion regulation. Moreover, these highly specific Cu^{2+} chelators can be applied as chemical tools to modulate Cu homeostatic pathways and Cu induced oxidative stress response in neurodegenerative conditions like Alzheimer's disease and in Cu-overload disorders like Wilson's disease. Finally, the molecular design of the Cu^{2+} binders, synthesized *via* a simple modular strategy, can serve as scaffolds for design and development of molecules aimed at chelation therapy for Cu-overload induced diseases.

Animal ethics statement

Zebrafish were bred and maintained and experiments were performed in accordance with guidelines and protocols approved by the institutional animal ethics committee of the Tata Institute of Fundamental Research.

Conflicts of interest

There are no conflicts to declare.

Acknowledgements

A. D. acknowledges financial support from TIFR and Department of Atomic Energy, India. The authors acknowledge Prof. Michael J. Petris for generously sharing MEF Atp7a$^{-/-}$ cells; Dr Marion Kerscher for her help with the illustration of MOMEC optimized structures and Dr Sreelaja Nair for helpful discussions on zebrafish larvae results. The authors acknowledge Cell culture and Imaging facility, Department of Chemical Sciences, TIFR, India; National NMR facility, TIFR, India; Electron spin resonance laboratory, Department of Chemical Sciences, TIFR; Biophotonics Laboratory, Department of Chemical Sciences, TIFR; and Mass Laboratory, Chemistry Department, Indian Institute of Technology, Bombay, India.

Notes and references

1 C. J. Chang, *Nat. Chem. Biol.*, 2015, **11**, 744–747.
2 M. J. Daly, E. K. Gaidamakova, V. Y. Matrosova, A. Vasilenko, M. Zhai, A. Venkateswaran, M. Hess, M. V. Omelchenko, H. M. Kostandarithes, K. S. Makarova, L. P. Wackett, J. K. Fredrickson and D. Ghosal, *Science*, 2004, **306**, 1025–1028.
3 K. Barnese, E. B. Gralla, J. S. Valentine and D. E. Cabelli, *Proc. Natl. Acad. Sci. U. S. A.*, 2012, **109**, 6892–6897.
4 Y. Hatori, Y. Yan, K. Schmidt, E. Furukawa, N. M. Hasan, N. Yang, C.-N. Liu, S. Sockanathan and S. Lutsenko, *Nat. Commun.*, 2016, **7**, 10640.
5 M. L. Schlief, T. West, A. M. Craig, D. M. Holtzman and J. D. Gitlin, *Proc. Natl. Acad. Sci. U. S. A.*, 2006, **103**, 14919–14924.
6 A. I. Bush, C. L. Masters and R. E. Tanzi, *Proc. Natl. Acad. Sci. U. S. A.*, 2003, **100**, 11193–11194.
7 E. Gaggelli, H. Kozlowski, D. Valensin and G. Valensin, *Chem. Rev.*, 2006, **106**, 1995–2044.
8 S. Lutsenko, *Curr. Opin. Chem. Biol.*, 2010, **14**, 211–217.
9 I. Fridovich, *Science*, 1978, **201**, 875–880.
10 Q. Liu, U. Berchner-Pfannschmidt, U. Möller, M. Brecht, C. Wotzlaw, H. Acker, K. Jungermann and T. Kietzmann, *Proc. Natl. Acad. Sci. U. S. A.*, 2004, **101**, 4302–4307.
11 B. Halliwell and J. M. Gutteridge, *Biochem. J.*, 1984, **219**, 1–14.
12 S. J. Stohs and D. Bagchi, *Free Radical Biol. Med.*, 1995, **18**, 321–336.
13 K. Jomova and M. Valko, *Toxicology*, 2011, **283**, 65–87.
14 L. Macomber and J. A. Imlay, *Proc. Natl. Acad. Sci. U. S. A.*, 2009, **106**, 8344–8349.
15 M. F. Poyton, A. M. Sendecki, X. Cong and P. S. Cremer, *J. Am. Chem. Soc.*, 2016, **138**, 1584–1590.

16 B. C. Dickinson and C. J. Chang, *Nat. Chem. Biol.*, 2011, **7**, 504–511.
17 L. K. Charkoudian, D. M. Pham and K. J. Franz, *J. Am. Chem. Soc.*, 2006, **128**, 12424–12425.
18 T. Storr, M. Merkel, G. X. Song-Zhao, L. E. Scott, D. E. Green, M. L. Bowen, K. H. Thompson, B. O. Patrick, H. J. Schugar and C. Orvig, *J. Am. Chem. Soc.*, 2007, **129**, 7453–7463.
19 Y. Wei and M. Guo, *Angew. Chem., Int. Ed.*, 2007, **46**, 4722–4725.
20 M. R. Jones, E. Mathieu, C. Dyrager, S. Faissner, Z. Vaillancourt, K. J. Korshavn, M. H. Lim, A. Ramamoorthy, V. Wee Yong, S. Tsutsui, P. K. Stys and T. Storr, *Chem. Sci.*, 2017, **8**, 5636–5643.
21 K. J. Franz, *Curr. Opin. Chem. Biol.*, 2013, **17**, 143–149.
22 M. Eckshtain-Levi, R. Lavi, D. S. Yufit, B. Daniel, O. Green, O. Fleker, M. Richman, S. Rahimipour, A. Gruzman and L. Benisvy, *Chem. Commun.*, 2016, **52**, 2350–2353.
23 A. Robert, Y. Liu, M. Nguyen and B. Meunier, *Acc. Chem. Res.*, 2015, **48**, 1332–1339.
24 A. Roberts Eve and L. Schilsky Michael, *Hepatology*, 2008, **47**, 2089–2111.
25 V. Prachayasittikul, S. Prachayasittikul, S. Ruchirawat and V. Prachayasittikul, *Drug Des., Dev. Ther.*, 2013, **7**, 1157–1178.
26 P. Leanderson and C. Tagesson, *Carcinogenesis*, 1996, **17**, 545–550.
27 X. Ding, H. Xie and Y. J. Kang, *J. Nutr. Biochem.*, 2011, **22**, 301–310.
28 A. J. Baxter and E. P. Krenzelok, *Clin. Toxicol.*, 2008, **46**, 1083–1084.
29 C. Cheignon, P. Faller, D. Testemale, C. Hureau and F. Collin, *Metallomics*, 2016, **8**, 1081–1089.
30 M. A. Greenough, A. Ramirez Munoz, A. I. Bush and C. M. Opazo, *Metallomics*, 2016, **8**, 831–839.
31 P. Faller, C. Hureau and O. Berthoumieu, *Inorg. Chem.*, 2013, **52**, 12193–12206.
32 D. Pramanik, C. Ghosh and S. G. Dey, *J. Am. Chem. Soc.*, 2011, **133**, 15545–15552.
33 J. P. Taylor, R. H. Brown Jr and D. W. Cleveland, *Nature*, 2016, **539**, 197–206.
34 S. Sangwan, A. Zhao, K. L. Adams, C. K. Jayson, M. R. Sawaya, E. L. Guenther, A. C. Pan, J. Ngo, D. M. Moore, A. B. Soriaga, T. D. Do, L. Goldschmidt, R. Nelson, M. T. Bowers, C. M. Koehler, D. E. Shaw, B. G. Novitch and D. S. Eisenberg, *Proc. Natl. Acad. Sci. U. S. A.*, 2017, **114**, 8770–8775.
35 J. S. Valentine and P. J. Hart, *Proc. Natl. Acad. Sci. U. S. A.*, 2003, **100**, 3617–3622.
36 N. Fujimaki, F. Kitamura and H. Takeuchi, *Biochemistry*, 2013, **52**, 5184–5194.
37 P. M. Roos, O. Vesterberg, T. Syversen, T. P. Flaten and M. Nordberg, *Biol. Trace Elem. Res.*, 2013, **151**, 159–170.
38 S. Ishida, P. Andreux, C. Poitry-Yamate, J. Auwerx and D. Hanahan, *Proc. Natl. Acad. Sci. U. S. A.*, 2013, **110**, 19507–19512.
39 A. Gupte and R. J. Mumper, *Cancer Treat. Rev.*, 2009, **35**, 32–46.
40 Y. Wang, S. Zhu, G. A. Weisman, J. D. Gitlin and M. J. Petris, *PLoS One*, 2012, **7**, e43039.
41 A. Bhattacharjee, H. Yang, M. Duffy, E. Robinson, A. Conrad-Antoville, Y.-W. Lu, T. Capps, L. Braiterman, M. Wolfgang, M. P. Murphy, L. Yi, S. G. Kaler, S. Lutsenko and M. Ralle, *J. Biol. Chem.*, 2016, **291**, 16644–16658.
42 R. Linz and S. Lutsenko, *J. Bioenerg. Biomembr.*, 2007, **39**, 403–407.
43 E. V. Polishchuk, M. Concilli, S. Iacobacci, G. Chesi, N. Pastore, P. Piccolo, S. Paladino, D. Baldantoni, S. C. D. van Ijzendoorn, J. Chan, C. J. Chang, A. Amoresano, F. Pane, P. Pucci, A. Tarallo, G. Parenti, N. Brunetti-Pierri, C. Settembre, A. Ballabio and R. S. Polishchuk, *Dev. Cell*, 2014, **29**, 686–700.
44 M. L. Graper, D. Huster, S. G. Kaler, S. Lutsenko, M. L. Schilsky and D. J. Thiele, *Ann. N. Y. Acad. Sci.*, 2014, **1314**, v–vi.
45 L. A. Finney and T. V. Halloran, *Science*, 2003, **300**, 931–936.
46 A. W. Foster, R. Pernil, C. J. Patterson, A. J. P. Scott, L.-O. Palsson, R. Pal, I. Cummins, P. T. Chivers, E. Pohl and N. J. Robinson, *Nat. Chem. Biol.*, 2017, **13**, 409–414.
47 A. Hong-Hermesdorf, M. Miethke, S. D. Gallaher, J. Kropat, S. C. Dodani, J. Chan, D. Barupala, D. W. Domaille, D. I. Shirasaki, J. A. Loo, P. K. Weber, J. Pett-Ridge, T. L. Stemmler, C. J. Chang and S. S. Merchant, *Nat. Chem. Biol.*, 2014, **10**, 1034–1042.
48 L. Banci, I. Bertini, S. Ciofi-Baffoni, T. Kozyreva, K. Zovo and P. Palumaa, *Nature*, 2010, **465**, 645–648.
49 A. K. Boal and A. C. Rosenzweig, *Chem. Rev.*, 2009, **109**, 4760–4779.
50 J. J. A. Cotruvo, A. T. Aron, K. M. Ramos-Torres and C. J. Chang, *Chem. Soc. Rev.*, 2015, **44**, 4400–4414.
51 L. Yang, R. McRae, M. M. Henary, R. Patel, B. Lai, S. Vogt and C. J. Fahrni, *Proc. Natl. Acad. Sci. U. S. A.*, 2005, **102**, 11179–11184.
52 M. C. Linder, *Mutat. Res.*, 2001, **475**, 141–152.
53 B. Alies, E. Renaglia, M. Rózga, W. Bal, P. Faller and C. Hureau, *Anal. Chem.*, 2013, **85**, 1501–1508.
54 S. Rabizadeh, E. B. Gralla, D. R. Borchelt, R. Gwinn, J. S. Valentine, S. Sisodia, P. Wong, M. Lee, H. Hahn and D. E. Bredesen, *Proc. Natl. Acad. Sci. U. S. A.*, 1995, **92**, 3024–3028.
55 P. Delangle and E. Mintz, *Dalton Trans.*, 2012, **41**, 6359–6370.
56 E. L. Que, D. W. Domaille and C. J. Chang, *Chem. Rev.*, 2008, **108**, 1517–1549.
57 S. Jia, K. M. Ramos-Torres, S. Kolemen, C. M. Ackerman and C. J. Chang, *ACS Chem. Biol.*, 2017, **13**, 1844–1852.
58 K. Harry and J. D. Spivack, *US Pat.*, No. US2928876, 1960.
59 Q. Wang and K. J. Franz, *Bioorg. Med. Chem. Lett.*, 2017, **27**, 4165–4170.
60 E. Faggi, R. Gavara, M. Bolte, L. Fajarí, L. Juliá, L. Rodríguez and I. Alfonso, *Dalton Trans.*, 2015, **44**, 12700–12710.
61 M. Tarnai, PhD thesis, Heidelberg University, 2006.
62 S. Y. Ebrahimipour, I. Sheikhshoaie, J. Castro, W. Haase, M. Mohamadi, S. Foro, M. Sheikhshoaie and S. Esmaeili-Mahani, *Inorg. Chim. Acta*, 2015, **430**, 245–252.

63 P. Comba, T. W. Hambley and B. Martin, in *Molecular Modeling of Inorganic Compounds*, Wiley-VCH Verlag GmbH & Co. KGaA, 3rd edn with a tutorial, based on MOMEC3, 2009, pp. 215–292.
64 P. Comba, M. Ströhle and T. W. Hambley, *Helv. Chim. Acta*, 1995, **78**, 2042–2047.
65 P. Comba, B. Martin and A. Sanyal, *J. Comput. Chem.*, 2013, **34**, 1598–1608.
66 J. E. Bol, C. Buning, P. Comba, J. Reedijk and M. Ströhle, *J. Comput. Chem.*, 1998, **19**, 512–523.
67 P. V. Bernhardt and P. Comba, *Inorg. Chem.*, 1992, **31**, 2638–2644.
68 M. G. D. Leed, N. Wolkow, D. M. Pham, C. L. Daniel, J. L. Dunaief and K. J. Franz, *J. Inorg. Biochem.*, 2011, **105**, 1161–1172.
69 J. Marks, I. Pozdnyakova, J. Guidry and P. Wittung-Stafshede, *J. Biol. Inorg. Chem.*, 2004, **9**, 281–288.
70 O. Farver and I. Pecht, *Coord. Chem. Rev.*, 2011, **255**, 757–773.
71 L. G. Sillen and A. E. Martell, *Stability Constants of Metal Ion Complexes*, Chemical Society, 17th edn, 1964.
72 B. Halliwell, J. M. C. Gutteridge and O. I. Aruoma, *Anal. Biochem.*, 1987, **165**, 215–219.
73 E. Farkas, É. A. Enyedy and H. Csóka, *Polyhedron*, 1999, **18**, 2391–2398.
74 A. I. B. Romo, D. S. Abreu, T. d. F. Paulo, M. S. P. Carepo, E. H. S. Sousa, L. Lemus, C. Aliaga, A. A. Batista, O. R. Nascimento, H. D. Abruña and I. C. N. Diógenes, *Chem.–Eur. J.*, 2016, **22**, 10081–10089.
75 N. Berthet, V. Martel-Frachet, F. Michel, C. Philouze, S. Hamman, X. Ronot and F. Thomas, *Dalton Trans.*, 2013, **42**, 8468–8483.
76 Y. Ma, T. Ogino, T. Kawabata, J. Li, K. Eguchi and S. Okada, *Free Radical Biol. Med.*, 1999, **27**, 227–233.
77 Y. Ma, L. Cao, T. Kawabata, T. Yoshino, B. B. Yang and S. Okada, *Free Radical Biol. Med.*, 1998, **25**, 568–575.
78 J. Zheng, J. R. Lou, X.-X. Zhang, D. M. Benbrook, M. H. Hanigan, S. E. Lind and W.-Q. Ding, *Cancer Lett.*, 2010, **298**, 186–194.
79 P. A. Castro, A. Ramirez, F. J. Sepúlveda, C. Peters, H. Fierro, J. Waldron, S. Luza, J. Fuentealba, F. J. Muñoz, G. V. De Ferrari, A. I. Bush, L. G. Aguayo and C. M. Opazo, *Front. Aging Neurosci.*, 2014, **6**, 319.
80 P. Chavez-Crooker, N. Garrido and G. A. Ahearn, *J. Exp. Biol.*, 2001, **204**, 1433–1444.
81 V. Mugoni, A. Camporeale and M. M. Santoro, *J. Visualized Exp.*, 2014, **89**, 51328.
82 R. Squitti, P. M. Rossini, E. Cassetta, F. Moffa, P. Pasqualetti, M. Cortesi, A. Colloca, L. Rossi and A. Finazzi-Agro', *Eur. J. Clin. Invest.*, 2002, **32**, 51–59.
83 A. Barzegar and A. A. Moosavi-Movahedi, *PLoS One*, 2011, **6**, 26012.
84 Y. Aboul-Enein Hassan, I. Kruk, A. Kładna, K. Lichszteld and T. Michalska, *Biopolymers*, 2007, **86**, 222–230.
85 G. Yücel, Z. Zhao, I. El-Battrawy, H. Lan, S. Lang, X. Li, F. Buljubasic, W.-H. Zimmermann, L. Cyganek, J. Utikal, U. Ravens, T. Wieland, M. Borggrefe, X.-B. Zhou and I. Akin, *Sci. Rep.*, 2017, **7**, 2935.
86 A. Ngkelo, K. Meja, M. Yeadon, I. Adcock and P. A. Kirkham, *J. Inflammation*, 2012, **9**, 1.
87 C. White, J. Lee, T. Kambe, K. Fritsche and M. J. Petris, *J. Biol. Chem.*, 2009, **284**, 33949–33956.
88 M. Priyadarshini, L. A. Orosco and P. J. Panula, *PLoS One*, 2013, **8**, 81851.
89 R. Zhang, J. Zhao, G. Han, Z. Liu, C. Liu, C. Zhang, B. Liu, C. Jiang, R. Liu, T. Zhao, M.-Y. Han and Z. Zhang, *J. Am. Chem. Soc.*, 2016, **138**, 3769–3778.
90 S. Wu, G. Ji, J. Liu, S. Zhang, Y. Gong and L. Shi, *Environ. Toxicol.*, 2016, **31**, 1241–1249.
91 J. L. Anderson, J. D. Carten and S. A. Farber, in *Methods. Cell. Biol.*, ed. H. W. Detrich, M. Westerfield and L. I. Zon, Academic Press, 2016, vol. 133, pp. 165–178.
92 L. Fang and Y. I. Miller, *Free Radical Biol. Med.*, 2012, **53**, 1411–1420.
93 M. E. Hahn, A. G. McArthur, S. I. Karchner, D. G. Franks, M. J. Jenny, A. R. Timme-Laragy, J. J. Stegeman, B. R. Woodin, M. J. Cipriano and E. Linney, *PLoS One*, 2014, **9**, 113158.
94 Q. Wang, X. Tan, S. Jiao, F. You and P.-J. Zhang, *PLoS One*, 2014, **9**, 102492.
95 M. Hagedorn, M. McCarthy, V. L. Carter and S. A. Meyers, *PLoS One*, 2012, **7**, 39397.
96 A. Roberts, B. Bill and D. Glanzman, *Front. Neural Circuits*, 2013, **7**, 126.
97 R. C. Eaton, R. K. K. Lee and M. B. Foreman, *Prog. Neurobiol.*, 2001, **63**, 467–485.
98 M. H. Green, R. K. Ho and M. E. Hale, *J. Exp. Biol.*, 2011, **214**, 3111–3123.
99 H. A. Field, K. A. Kelley, L. Martell, A. M. Goldstein and F. C. Serluca, *Neurogastroenterol. Motil.*, 2009, **21**, 304–312.
100 W. Mo, F. Chen, A. Nechiporuk and T. Nicolson, *BMC Neurosci.*, 2010, **11**, 110.
101 V. Romanello and M. Sandri, *Front. Physiol.*, 2015, **6**, 422.
102 E. Cadenas, *Mol. Aspects Med.*, 2004, **25**, 17–26.
103 E. J. Anderson and P. D. Neufer, *Am. J. Physiol. Cell Physiol.*, 2006, **290**, C844–C851.
104 C. M. Ackerman and C. J. Chang, *J. Biol. Chem.*, 2018, **13**, 4628–4635.
105 C. J. Chang, *Acc. Chem. Res.*, 2017, **50**, 535–538.